Sensors and Materials, Vol. 38, No. 11 (2026) 6401–6414
MYU Tokyo

S & M 4687

Development of Bendable Ultrasonic Scalpel with Grasping Mechanism Using Superelastic Alloy Active Blade

Daisuke Haraguchi[1*] and Ryoga Ono[2]

[1]Faculty of Science and Engineering, Kindai University, 3-4-1 Kowakae, Higashiosaka, Osaka 577-8502, Japan
[2]Toyohashi University of Technology, 1-1 Hibarigaoka, Tenpaku, Toyohashi, Aichi 441-8580, Japan

(Received July 14, 2026; accepted August 25, 2026)

Keywords: ultrasonic scalpel, flexible joint, superelastic alloy, grasping mechanism, robotic surgical instrument

In this study, we developed a multi-degree-of-freedom (multi-DOF) ultrasonic scalpel equipped with a superelastic alloy (NiTi) active blade that enables both tip bending and grasping motions. The active blade features a strip-shaped localized flexible section to facilitate compact bending, while a multistage hinge-based wire-driven mechanism achieves a bending range of ±60°. A blade-straddling single-moving-jaw grasping mechanism was also incorporated to provide grasping capability within the limited 8 mm outer diameter without interfering with the centrally routed active blade. The ultrasonic transducer can be easily detached from the active blade and replaced. A prototype device was fabricated on the basis of an active-blade design obtained by estimating the blade's ultrasonic resonance using the finite element method, and its fundamental performance was evaluated through excitation experiments and noncontact 3D vibration measurements. In the straight, unloaded posture, the active blade exhibited a resonant frequency of 57.5 kHz and a transducer current of 528 mA at a driving voltage of 25 V. Stable ultrasonic resonance was maintained even in the bent state; however, vibration amplitude attenuation and durability issues were identified as major challenges. In cauterization experiments using an edible porcine meat sample, the grasping mechanism enabled effective wide-area cauterization in the straight posture, whereas sufficient cauterization was not achieved when the tip was bent.

1. Introduction

In recent years, the number of minimally invasive surgical procedures using endoscopes has continued to increase annually. Furthermore, the proliferation of robot-assisted surgery necessitates highly precise treatment techniques, making the development of multi-degree-of-freedom (multi-DOF) surgical instruments a critical technological focus that is being actively researched.[1–4] An ultrasonic coagulation and incision device (ultrasonic scalpel) is a surgical instrument that simultaneously performs coagulation and incision by applying ultrasonic vibration to its treatment part (active blade), generating frictional heat within the tissue. This

*Corresponding author: e-mail: d.haraguchi@mech.kindai.ac.jp
https://doi.org/10.18494/SAM6528

ISSN 0914-4935 © MYU K.K.
https://myukk.org/

frictional heat coagulates proteins, while the physical friction cuts the tissue. Compared with electrocautery scalpels, ultrasonic devices are better suited for delicate procedures. Because they allow surgeons to perform simultaneous incisions and coagulations rapidly and with minimal blood loss,[5,6] ultrasonic scalpels have become indispensable energy devices in many surgical procedures. Consequently, providing these devices with multi-DOF capabilities is strongly desired to enable more precise and safer operations.

Many research groups have attempted to develop multi-DOF ultrasonic scalpels. Choi *et al.* developed a small transducer to miniaturize the instrument.[7] Ogura *et al.* and Khalaji *et al.* developed 2-DOF ultrasonic scalpels by placing a miniature transducer at the tip of a bendable joint.[8,9] Subsequently, Hasuo *et al.* added a grasping function to the device developed by Ogura *et al*., and Ogura *et al.* later introduced a highly functional multi-DOF scalpel featuring both 2-DOF bending and grasping mechanisms.[8,10,11] Kobayashi *et al.* proposed an ultrasonic scalpel with 1-DOF bending and 1-DOF rotation driven by an ultrasonic motor.[12] In all these devices, locating the miniaturized transducer at the movable joint's tip helps maintain treatment performance. However, their outer diameters are typically 10–13 mm or larger (compared with 5 mm for standard handheld instruments and 8 mm for standard robotic instruments), and their bending sections are relatively long. This makes miniaturization difficult and renders them unsuitable for precision surgery in confined spaces. Furthermore, placing the transducer inside the patient's body poses significant challenges regarding sterilization, cleaning, electrical safety, and cost in practical use.

Conversely, Hashimoto *et al.* and Wakako and Hashimoto positioned the ultrasonic transducer at the base of the instrument (outside the body) and utilized a superelastic alloy (NiTi) wire as the active blade to transmit vibrations.[13–15] On the basis of this approach, they developed an ultrasonic scalpel with a thin tip probe capable of 1-DOF bending on one side via a linkage mechanism. However, this device featured only a simple probe without a grasping mechanism, which is necessary for effective and wide-area tissue coagulation and incision. Additionally, its bending link mechanism required substantial spatial clearance during flexion, leaving issues to be resolved for broader surgical applications.

Recent studies have continued to address the miniaturization, articulation, and flexibility of ultrasonic surgical devices for minimally invasive and robotic surgery. Cao *et al.* developed a miniature Langevin ultrasonic transducer toward the aim of fabricating an ultrasonic scalpel for single-port robotic surgery, indicating that the miniaturization of ultrasonic energy devices remains an important issue in robotic surgical instrumentation.[16] Wang *et al.* modeled a curved-waveguide ultrasonic scalpel to improve surgical flexibility for intricate procedures, suggesting that ultrasonic wave transmission through a curved or articulated structure is still an active research topic.[17] In addition, Wu *et al.* reviewed recent progress in flexible ultrasonic scalpels for minimally invasive surgery, further highlighting the continuing need for compact and flexible ultrasonic devices.[18] However, most existing approaches still involve a trade-off among maintaining ultrasonic vibration performance, achieving a compact articulated tip, and incorporating a grasping function within a small outer diameter.

To resolve these issues, in this study, we adopt a configuration where the ultrasonic transducer is placed outside the body (at the base of the instrument), utilizing a superelastic alloy

active blade to enable a compact, flexible bending motion at the tip while incorporating a grasping mechanism. In particular, experimental knowledge on how ultrasonic vibration propagates through a bendable active blade under different bending postures remains limited. Clarifying the three-dimensional vibration behavior of such a blade is important for identifying the causes of performance degradation and for establishing design guidelines for future bendable ultrasonic scalpels. We applied the design principles of a wire-driven flexible joint previously developed by Zhou *et al.* to the scalpel's tip mechanism and extended them to a compact ultrasonic scalpel mechanism that integrates a bendable active blade and a grasping function.[19]

The novel aspects and contributions of this study are as follows.

(1) Development of a superelastic alloy active blade with a localized flexible section that enables compact bending while transmitting ultrasonic vibration
(2) Development of a space-saving wire-driven tip mechanism that integrates both bending and grasping functions around the centrally routed active blade within an 8 mm outer diameter
(3) Experimental clarification of the three-dimensional ultrasonic vibration behavior of the active blade under different bending postures using noncontact 3D vibration measurements

The paper is organized as follows: Sect. 2 includes a description of the design of the wire-driven multi-DOF mechanism for the ultrasonic scalpel. In Sect. 3, details of the design of the superelastic alloy active blade, including the estimation of its ultrasonic resonance using the finite element method (FEM) and experimental verification through vibration measurements, are given. Section 4 concerns the ultrasonic excitation experiments using the assembled prototype. Simple cauterization experiments using an edible porcine meat sample to evaluate the basic treatment performance are described in Sect. 5. In Sect. 6, we discuss the findings, followed by the conclusions in Sect. 7.

2. Design of Multi-DOF Mechanism for Ultrasonic Scalpel

2.1 Overview of device design

In previous attempts to achieve multi-DOFs, the following methods were primarily proposed: (1) placing a miniature ultrasonic transducer at the tip to provide a 2-DOF system equipped with a grasping mechanism[11] and (2) positioning the transducer at the base and utilizing a superelastic alloy probe as an active blade to achieve a thin tip with 1-DOF bending on one side.[14] In the former approach, it is easier to maximize device performance; however, placing the transducer at the tip increases both the device diameter and the length of the bending section, making it unsuitable for precision surgery in confined spaces. In the latter approach, while the tip is successfully miniaturized and suitable for precision procedures, achieving multi-DOFs is difficult. In particular, the lack of an established design method for integrating a grasping mechanism remains a major challenge.

Assuming the use of the multi-DOF ultrasonic scalpel within a robot-assisted surgical system, we prioritize the advantages of a miniaturized and slim device tip and thereby adopted the method of placing the transducer at the base. We developed a novel superelastic alloy active blade that enables the bending motion of the device tip while successfully implementing a

grasping mechanism, which had not been realized in previous base-transducer designs. Figure 1 shows an overview of the designed ultrasonic scalpel [Fig. 1(a)] and a schematic of the multi-DOF wire-driven mechanism [Fig. 1(b)]. To match current robotic surgical forceps, the device's outer diameter is specified as 8 mm, and the tip features a 1-DOF flexure joint and a grasping mechanism. Bending and grasping are actuated by a total of four driving wires that operate independently without mutual interference. The design also ensures that they do not interfere with the active blade routed through the center of the device. The ultrasonic transducer utilizes a commercial component from a conventional portable ultrasonic scalpel, Sonicision™. The active blade made of the superelastic alloy NiTi can be directly screwed into this transducer, allowing it to be completely separated from the multi-DOF mechanism for easy attachment, detachment, and replacement. The active blade is supported at only three points—before and after the flexure joint, and at the base of the shaft—using soft silicone tubes to prevent metal-to-metal contact.

2.2 Tip bending and grasping mechanism

The tip mechanism was designed with an 8 mm outer diameter to suit precision procedures, making it the slimmest multi-DOF ultrasonic scalpel among those in previous studies. Figure 2 shows the mechanical design of the tip [Fig. 2(a)] and a photograph of the prototype [Fig. 2(b)]. The prototype achieves a bending range of ±60° at the flexure joint and a maximum grasping angle of 30°. A total of four twisted stainless-steel wires (0.35 mm outer diameter) were used for actuation, with stainless-steel pipes crimped at the ends to prevent loosening.

For the bending motion, a four-stage hinge mechanism forms the flexure joint, providing 1-DOF bending perpendicular to the grasping direction. Bending is actuated by antagonistically driving a pair of wires (green) routed through both sides inside the joint. Since the hinge

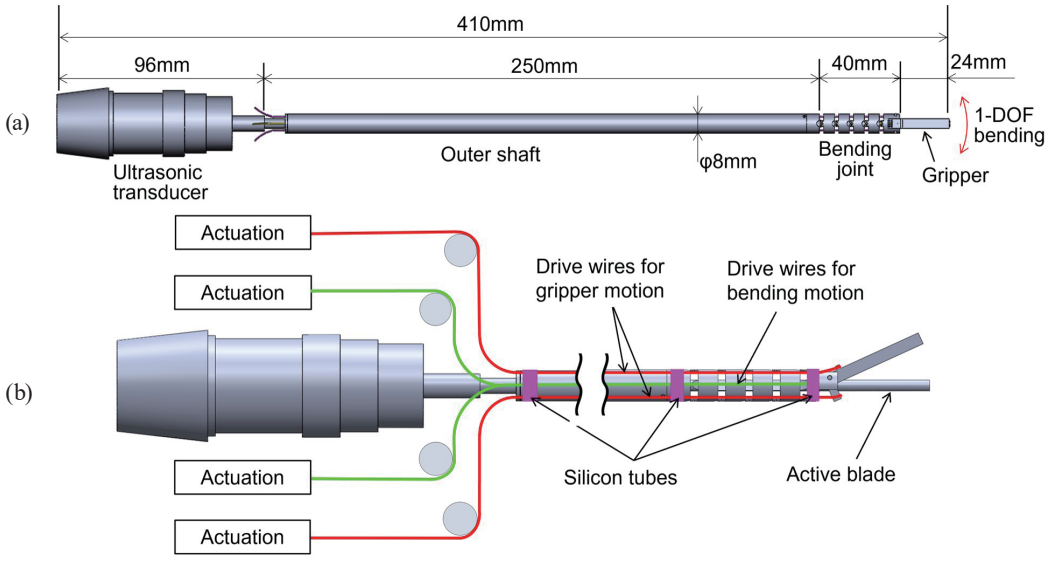
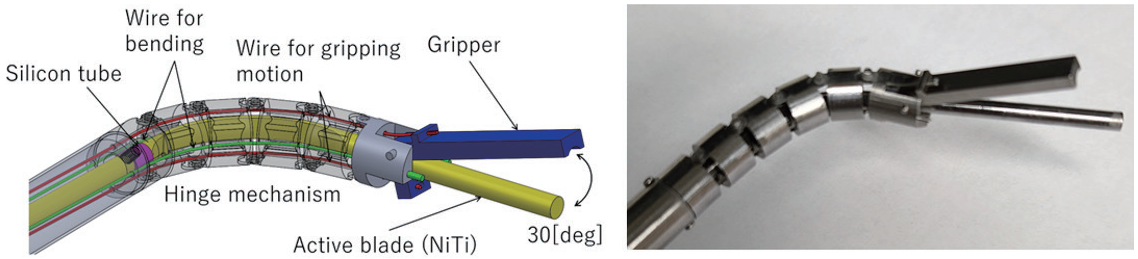


Fig. 1. (Color online) (a) Overview of the ultrasonic scalpel and (b) schematic of the multi-DOF wire-drive mechanism.



(a) (b)

Fig. 2. (Color online) (a) Mechanism design of the ultrasonic scalpel tip and (b) photograph of the prototype.

mechanism components are rigid bodies, unintended deformation outside the bending plane is minimized, and the direct tension load of the driving wires is prevented from being applied to the active blade inside the joint. Furthermore, the superelastic-alloy active blade is flattened into a strip where it passes through the joint, providing localized flexibility in the bending direction while maintaining out-of-plane rigidity to ensure structural strength.

To enhance the device performance, a single-moving-jaw grasping mechanism was integrated into the tip. Drive wires (red) are attached above and below the gripper rotation axis, allowing the jaw to open and close through antagonistic wire actuation. To avoid interference with the bending motion, these grasping wires pass directly under the rotation axis of the joint hinge mechanism. In addition, to generate sufficient grasping torque within the limited 8 mm outer diameter, the gripper component was designed with a clearance hole through which the centrally located active blade passes. This blade-straddling arrangement allows the grasping mechanism to utilize a larger portion of the outer diameter of the instrument, positioning the wire attachment points near the outer periphery and thereby increasing the effective moment arm about the gripper rotation axis.

3. Design of Bendable Ultrasonic Active Blade

3.1 Shape of superelastic-alloy active blade

Figure 3 illustrates the geometry of the designed superelastic-alloy active blade. The total length (317 mm) was determined via FEM analysis (described in the next section). The proximal shaft has an outer diameter of 4.0 mm—the maximum allowable size within the 8 mm outer sheath that avoids wire interference—ensuring efficient ultrasonic propagation. The proximal end is threaded for direct attachment to the vibration horn, minimizing vibration loss and allowing easy connection, disconnection, and replacement. The distal tip is slightly thinned (2.8 mm outer diameter) to amplify the vibration amplitude, while a 0.7-mm-thick strip section provides localized flexibility. This plate-like flexible section allows the active blade to bend smoothly and compactly to achieve multi-DOFs. The leading edge of the blade (treatment section) is longer than a half-wavelength of ultrasonic wave propagation (approximately 28 mm) to ensure that a vibration antinode is reliably generated in this section.

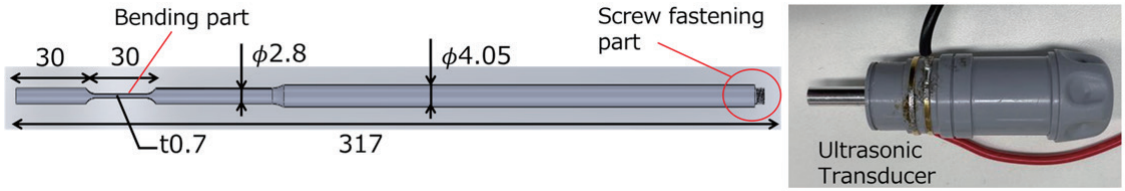


Fig. 3. (Color online) Shape of the superelastic-alloy active blade.

3.2 Estimation of ultrasonic resonance using FEM

To determine the precise dimensions and shape of the active blade, the modal analysis of its FEM model was performed using Ansys software. In this study, because longitudinal resonance is critical and analyzing other areas is difficult owing to fixture constraints, the analysis was focused on resonance frequencies, wavelengths, and total length. Table 1 shows the material properties and analysis results. The total blade length was adjusted so that the longitudinal vibration eigenmodes align with the transducer's 55–56 kHz resonant frequency. Figure 4 shows the longitudinal wave resonance mode shapes and corresponding stress distributions. A vibration node (where displacement is negligible) appears approximately 10 mm from the blade tip; it is desirable for this point to be as close to the blade root as possible. Because the plate section has the lowest stiffness, the vibration amplitude is maximized in this area, resulting in high stress concentrations.

The validity of the FEM results can be verified using the fundamental equation for the speed of sound in a medium:

$$\lambda = \frac{1}{f}\sqrt{\frac{E}{\rho}}, \tag{1}$$

where λ is the wavelength, f is the frequency, E is Young's modulus, and ρ is the density. Using Eq. (1), the theoretical wavelength at the resonant frequency is calculated to be approximately 52.4 mm, which closely matches the 56.5 mm wavelength derived from the FEM analysis. Given that the simplified Eq. (1) assumes a simple rod shape, this value is reasonably close to the FEM result, confirming the validity of the analysis. This accuracy is further supported by the experimental verification described in the next section.

3.3 Verification of ultrasonic resonance of the active blade

The designed active blade was connected to the transducer, and ultrasonic excitation was performed in an unconstrained state to measure its resonant frequency and verify the design. The experimental setup is shown in Fig. 5. A bolt-clamped Langevin-type transducer (BLT) controller (M-5107W, MESS-TEK Co., Ltd.) equipped with a resonance tracking circuit was used to apply a sinusoidal voltage to the transducer. The driving voltage and current can be

Table 1
Material parameters and FEM settings and results for the active blade.

Material		NiTi	
Physical characteristics	Density	Young's modulus	Poisson ratio
	6500 kg/m^3	55 GPa	0.34
FEM settings and results	Natural frequency	55.286 kHz	
	Wavelength	56.5 mm	
	Mesh size	1.0 mm	
	Number of nodes	44140	



Fig. 4. (Color online) FEM analysis of ultrasonic resonance modes and stress distribution in the active blade.

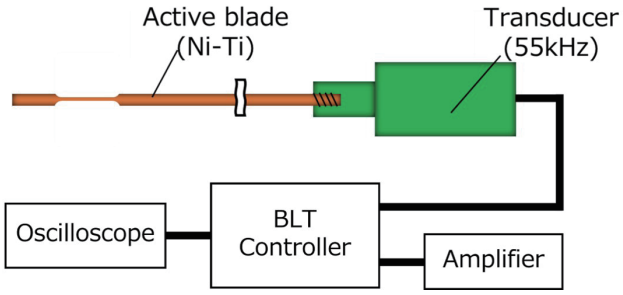


Fig. 5. (Color online) Equipment configuration for ultrasonic vibration.

monitored using an oscilloscope. Because the current correlates with vibration velocity, it serves as an evaluation index for vibration amplitude at a constant frequency.

The measured resonant frequency was 57.5 kHz, with a transducer current of 528 mA at a driving voltage of 25 V. Although the frequency slightly deviated from the FEM prediction (approximately 55.5 kHz), the baseline characteristics generally met the design targets. The design accuracy can be further enhanced by updating the material parameters of the FEM model on the basis of these experimental results. For comparison, the commercial Sonicision™ device exhibited a resonant frequency of 55.5 kHz and a current of 482 mA at 25 V. Although a

comprehensive evaluation of vibration transmissibility is necessary because of the different blade materials (titanium alloy for Sonicision), our NiTi active blade baseline vibration performance in a straight, unloaded state is considered reasonable and valid.

3.4 Measurement of vibration state at ultrasonic resonance

Next, the vibration state of the active blade at resonance was measured. The experimental setup is shown in Fig. 6(a). A noncontact 3D vibration measurement system consisting of three scanning laser Doppler vibrometers (PSV QTec, Polytec GmbH) enables simultaneous multipoint measurement. As shown in Fig. 6(b), the base of the active blade (transducer and connection) was fixed in a jig, and sleeves were attached before and after the flexible plate section. The tip was flexed by pulling a wire to evaluate changes in resonance across different bending angles. In the coordinate system, the longitudinal direction corresponds to the Y-axis. Flexion was oriented obliquely upward to facilitate laser beam irradiation.

Table 2 shows the measured resonance frequencies and triaxial vibration displacements (maximum value of the resonance component) at bending angles of 0, 15, and 30°. In this

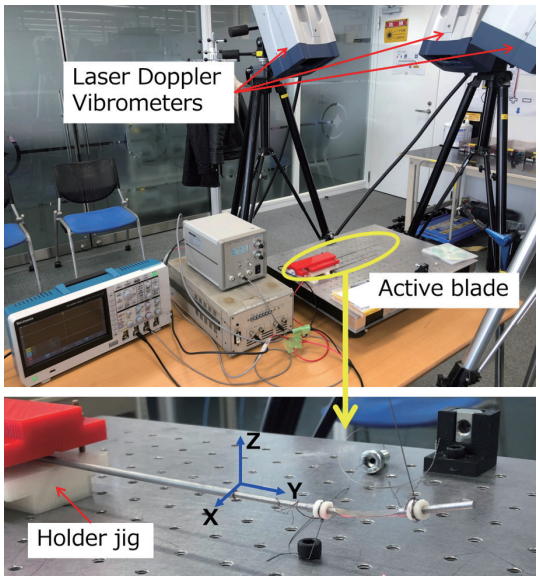


Fig. 6. (Color online) Experimental apparatus for noncontact 3D measurement of ultrasonic vibration.

Table 2
Results of three-dimensional ultrasonic vibration measurement with tip bending of the active blade.

Applied voltage (V)	Bending angle (deg)	Natural frequency (kHz)	Current (mA)	Tip displacement *X* (μm)	Tip displacement *Y* (μm)	Tip displacement *Z* (μm)
20	0	62.6	256	0.01	1.5	0.01
	15	62.6	184	0.02	1.2	0.01
	30	62.2	120	0.2	0.7	0.4

experiment, the resonant frequency shifted to 62–63 kHz, deviating significantly from the nominal frequency of 57.5 kHz. Notably, the constrained straight configuration already exhibited a resonant frequency of 62.6 kHz, and the frequency remained within 62.2–62.6 kHz as the bending angle increased to 30°. This indicates that the frequency shift was caused primarily by the mounting conditions rather than by blade bending or increased wire tension. Unlike the approximately unconstrained condition in Sect. 3.3, the holder jig and sleeves introduced finite-width mechanical constraints that did not necessarily coincide with the longitudinal vibration nodes. These constraints provided an additional stiffness path to the stationary frame and altered the coupled resonance of the transducer–blade system. Accordingly, the specific resonance of 62–63 kHz is considered dependent on the present experimental fixture. Even under the constraint conditions, stable ultrasonic resonance was maintained across all bending angles, and the frequency remained nearly constant. Regarding the tip displacement, the longitudinal amplitude (*Y*-axis component) decreased as the bending angle increased.

Conversely, transverse displacements (*X* and *Z* components) increased, indicating that the propagation direction of the longitudinal vibration shifted along the blade's curve. However, as reflected by the decrease in transducer current, the longitudinal wave amplitude attenuates with flexion. For instance, the 3D displacement vector magnitude at 30° bending was calculated to be approximately 0.83 μm, indicating a marked attenuation from the straight state.

Figure 7 displays the displacement distribution in the forward portion of the blade. The silhouette of the active blade is emphasized for clarity. The amplitude reaches its maximum at the flexible plate section, suggesting that high stress concentrations occur at the adjacent vibration nodes. Additionally, a node is observed near the leading edge of the blade, which aligns well with the FEM predictions. Similarly to the resonant frequency, the relative distribution of anti-nodes and nodes remains nearly constant regardless of the angle, though the local amplitudes decrease significantly as the overall blade flexion increases.

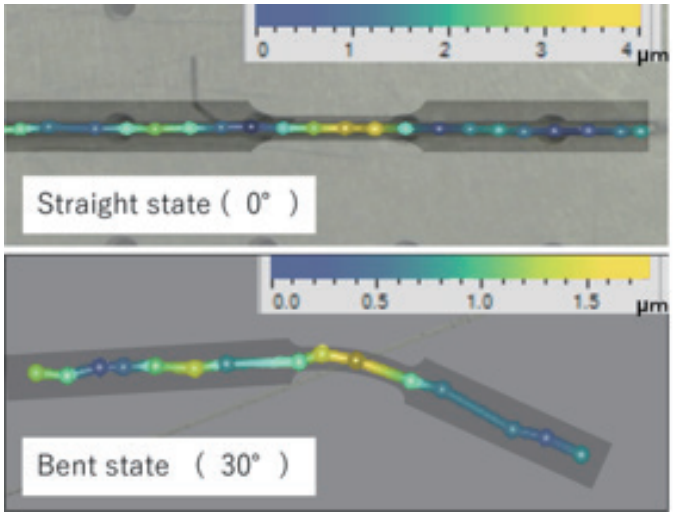


Fig. 7. (Color online) Displacement distribution of ultrasonic resonance (longitudinal wave component).

4. Vibration Experiment of Assembled Ultrasonic Scalpel

The developed active blade was integrated into the multi-DOF mechanism to evaluate resonance during wire-driven bending (Fig. 8). The driving wire was secured to a tensioner, and its tension was manually adjusted to flex the joint, followed by ultrasonic excitation using the configuration in Fig. 5.

The results (Table 3) show that a bending state of up to 60° was achieved, and the resonant frequency remained constant and stable across all angles. However, owing to the mounting-dependent resonance shift described in Sect. 3.4, the resonant frequency remained higher than the unconstrained value of 57.5 kHz. The transducer current decreased markedly as the bending angle increased. These results indicate that current compensation via the drive circuit is indispensable in ensuring consistent surgical performance regardless of the blade's posture.

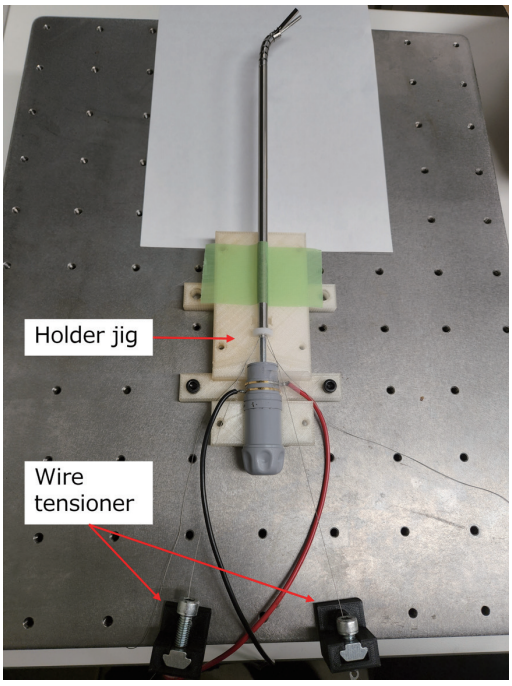


Fig. 8. (Color online) Experimental setup for ultrasonic scalpel excitation.

Table 3
Ultrasonic resonance of the assembled scalpel with tip bending.

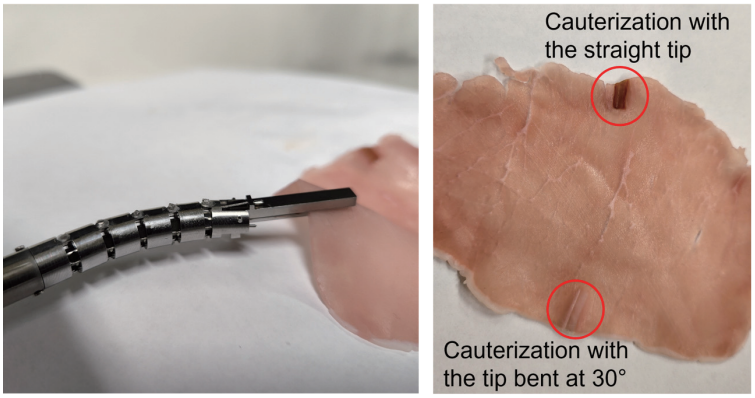
Applied voltage (V)	Bending angle (deg)	Natural frequency (kHz)	Current (mA)
20	0	62.5	282
	10	62.5	240
	20	62.5	190
	30	62.5	186
	40	62.5	166
	50	62.5	154
	60	62.5	130

5. Cauterization Experiment Using Edible Porcine Meat Sample

To evaluate the basic treatment performance of the prototype, cauterization experiments were conducted using an edible porcine meat sample (cured ham). This experiment was intended as a simple model of tissue coagulation and incision achieved using the grasping mechanism of an ultrasonic scalpel. Using the setup shown in Fig. 8, the sample was grasped between the active blade and the gripper, and a driving voltage of 45 V was applied to the transducer at the resonant frequency of 62.5 kHz for 10 s. The thermal denaturation of the grasped region was then visually inspected. Cauterization was tested with two tip postures: a straight tip posture and a 30°-flexed posture [Fig. 9(a)].

Figure 9(b) shows the cauterized regions after the experiment. In the straight posture, the treated area became blackened, indicating that sufficient heat was generated at the contact region between the blade and the sample. The grasping mechanism enabled a relatively wide contact area to be cauterized along the active blade. The transducer current during this experiment was 460 mA. In comparison, the commercial Sonicision™ device exhibited a transducer current of 473 mA under the same driving voltage of 45 V. These results suggest that the developed superelastic-alloy active blade has a baseline vibration performance comparable to that of a commercial ultrasonic scalpel in the straight, unloaded posture.

Conversely, when the tip was flexed at 30°, only slight white coagulation was observed in the treated region and the transducer current decreased to approximately 300 mA. The cured ham used in this experiment contained less moisture than living biological tissue, which may have made white denaturation difficult to observe. Nevertheless, the substantial decrease in transducer current and the limited cauterization observed in the flexed posture indicate that the longitudinal vibration of the blade was strongly attenuated by bending. In addition, after several repeated cauterization trials in the flexed posture, the active blade fractured at the flexible section. Therefore, both the vibration performance and durability of the blade in the bent state remain important issues to be addressed.



(a) (b)

Fig. 9. (Color online) Cauterization experiment of edible pork (cured ham).

6. Discussion

The design and experimental results obtained in this study provide several important findings regarding the feasibility and limitations of a bendable ultrasonic scalpel with a superelastic-alloy active blade.

First, the results indicate that an active blade with a localized flexible section can be designed by estimating its longitudinal resonance behavior using FEM. The threaded connection between the blade and the transducer horn provided stable ultrasonic resonance and also allowed the active blade to be easily attached, detached, and replaced. This modular configuration is advantageous for practical use because the active blade and the multi-DOF tip mechanism can be treated as separate components.

Second, the cauterization experiments also showed that the combination of the active blade and the grasping mechanism functioned effectively in the straight posture. Although the prototype blade tip had a simple round cross section, the treated area was broadly cauterized through contact with the grasped sample. Therefore, further improvement in treatment performance can be expected by optimizing the distal tip geometry, for example, by introducing a blade-like cross section suitable for ultrasonic coagulation and incision.

On the other hand, the reduction in vibration amplitude and the durability of the active blade in the bent posture remain major challenges. The decrease in vibration amplitude during bending can be attributed to two main factors: (1) energy loss associated with the change in the propagation direction of the longitudinal vibration along the curved blade and (2) vibration suppression caused by increased mechanical constraints at the blade supporting and bending mechanisms. Although the former is inherent to ultrasonic wave propagation through a continuously deformed structure, the latter can be mitigated by reducing the contact area of the blade supports, avoiding the axial loading of the blade during bending, and designing a housing that supports the transducer and shaft so as to minimize mechanical constraints. The mounting position should also be selected so that the transducer or shaft is supported as close as practicable to a longitudinal vibration node. Nevertheless, even with these measures, a mounting-dependent shift in resonant frequency may occur after integration into a robotic instrument, as indicated by the results in Sect. 3.4. Therefore, the drive circuit of a practical system should track the actual resonant frequency of the assembled system.

The fracture of the blade is considered to have been caused by stress concentration in the flexible section during ultrasonic excitation in the bent posture. Bending can excite transverse vibration components in addition to the intended longitudinal vibration, and regions where the blade stiffness or curvature changes abruptly tend to become vibration nodes. Such regions are therefore susceptible to local stress concentration. In the present prototype, the plate-like flexible section was designed to be as short as possible to prioritize compact bending. However, improving durability will require a longer flexible section with a larger radius of curvature, which would allow the blade to deform more gradually under a smaller constraint force. In addition to these geometric improvements, material-level approaches should also be investigated to improve the fatigue life of the NiTi active blade. In particular, the optimization of the heat-treatment conditions and the application of appropriate surface-finishing processes, such as

mechanical polishing or electropolishing, may reduce surface defects and suppress fatigue-crack initiation under combined bending and ultrasonic cyclic loading.

6.1 Limitations

This study was focused on the design of the active blade and the compact tip mechanism, as well as on the fundamental verification of ultrasonic resonance and cauterization performance. The drive or operation unit for the multi-DOF mechanism was not implemented as a specific system because various configurations are possible, including fully manual operation, a motorized actuator unit, or a detachable instrument for a surgical robot. In addition, the noncontact 3D vibration measurements described in Sect. 3.4 were limited to bending angles of up to 30° because the optical alignment of the laser beams became difficult at larger bending angles. Despite these limitations, the results demonstrated the basic feasibility of a multi-DOF ultrasonic scalpel using a superelastic-alloy active blade.

7. Conclusions

We demonstrated the feasibility of a bendable multi-DOF ultrasonic scalpel featuring a superelastic-alloy active blade. A plate-shaped local flexible section enabled compact wire-driven bending, and an integrated grasping mechanism allowed wide-area cauterization in the straight posture. Although stable ultrasonic resonance was maintained during bending, reduced cauterization performance due to vibration amplitude attenuation and blade durability were identified as key challenges. Future work will focus on improving the active blade geometry, developing a bending mechanism with lower constraint loads, refining the holding structure, and integrating an appropriate drive unit to enhance the overall performance of the ultrasonic scalpel.

Acknowledgments

This work was partly supported by JSPS KAKENHI Grant Number 20K14679. The authors are deeply grateful to Prof. Kentaro Nakamura of Tokyo Institute of Technology for his advice and the provision of experimental equipment. The authors are also deeply grateful to Mr. Morihito Hagura and Mr. Francois Bouteille of Polytec Japan K.K. for their help and support in using the 3D laser Doppler vibration measurement system. Finally, the authors would like to thank Ms. Miu Sato from the National Institute of Technology, Tokyo College, for her assistance with the experiments during her graduation research.

References

1 M. B. Hong and Y. H. Jo: IEEE/ASME Trans. Mechatron. **19** (2014) 500. https://doi.org/10.1109/TMECH.2013.2245143

2 M. Bazman, N. Yilmaz, and U. Tumerdem: Proc. 2018 IEEE 15th Int. Workshop on Advanced Motion Control (AMC, 2018) 153. https://doi.org/10.1109/AMC.2019.8371079

3 C. Forbrigger, A. Lim, O. Onaizah, S. Salmanipour, T. Looi, J. Drake, and E. Diller: IEEE Robot. Autom. Lett. **4** (2019) 1202. https://doi.org/10.1109/LRA.2019.2894504
4 F. Feng, W. Hong, and L. Xie: IEEE Access **8** (2020) 79573. https://doi.org/10.1109/ACCESS.2020.2991092
5 D. Gossot, G. Buess, A. Cuschieri, E. Leporte, M. Lirici, R. Marvik, D. Meijer, A. Melzer, and M. O. Schurr: Surg. Endosc. **13** (1999) 412. https://doi.org/10.1007/s004649901002
6 M. M. Fernández-Fernández, L. Montes-Jovellar, P. L. Parente Arias, and P. Ortega del Álamo: Eur. Arch. Otorhinolaryngol. **272** (2015) 3785. https://doi.org/10.1007/s00405-014-3423-6
7 W. Choi, R. Wang, E. Kobayashi, T. Ando, and I. Sakuma: Proc. 2014 Japan Society for Precision Engineering Autumn Conf. (JSPE, 2014) 79–80 (in Japanese). https://doi.org/10.11522/pscjspe.2014A.0_79
8 G. Ogura, R. Nakamura, Y. Muragaki, K. Takakura, and H. Iseki: Proc. The 2nd Joint Conference of The Society of Life Support Engineering (EAWLS, 2004) 239 (in Japanese). https://doi.org/10.5136/lifesupport.16.Supplement_239
9 I. Khalaji, M. D. Naish, and V. Patel: Proc. 2015 IEEE International Conference on Robotics and Automation (ICRA, 2015) 573. https://dx.doi.org/10.1109/ICRA.2015.7139236
10 T. Hasuo, G. Ogura, I. Sakuma, E. Kobayashi, H. Iseki, and R. Nakamura: J. Jpn. Soc. Comput. Aided Surg. **7** (2005) 313 (in Japanese). https://doi.org/10.5759/jscas1999.7.313
11 G. Ogura, R. Nakamura, Y. Muragaki, M. Hashizume, and H. Iseki: Surg. Endosc. **23** (2009) 2138. https://doi.org/10.1007/s00464-008-0248-7
12 E. Kobayashi, H. Sakamoto, W. Choi, T. Morita, T. Kanda, and I. Sakuma: Procedia CIRP **5** (2013) 70. https://doi.org/10.1016/j.procir.2013.01.014
13 M. Hashimoto, K. Bandou, and R. Wakako: J. Robot. Soc. Jpn. **24** (2006) 845 (in Japanese). https://doi.org/10.7210/jrsj.24.845
14 M. Hashimoto, K. Bandou, and R. Wakako: Proc. 2005 IEEE/RSJ Int. Conf. Intelligent Robots and Systems (IROS, 2005) 1742. https://doi.org/10.1109/IROS.2005.1545489
15 R. Wakako and M. Hashimoto: Proc. 2002 IEEE/RSJ Int. Conf. Intelligent Robots and Systems (IROS, 2002) 1415. https://doi.org/10.1109/IRDS.2002.1043953
16 Y. Cao, Y. Ding, C. Zhu, H. Kuang, R. Zhao, and K. Xu: Proc. 2024 IEEE Int. Conf. Advanced Intelligent Mechatronics (AIM, 2024) 853. https://doi.org/10.1109/AIM55361.2024.10636981
17 Y. Wang, S. Li, and Q. Xue: Proc. Inst. Mech. Eng. Part C: J. Mech. Eng. Sci. **238** (2024) 8819. https://doi.org/10.1177/09544062241248276
18 M. Wu, Q. Feng, S. Liu, and X. Lu: China Med. Devices **39** (2024) 156 (in Chinese). https://doi.org/10.3969/j.issn.1674-1633.2024.01.027
19 D. Zhou, K. Sanada, and D. Haraguchi: Sens. Mater. **32** (2020) 1027. https://doi.org/10.18494/SAM.2020.2655

About the Authors



Daisuke Haraguchi received his Ph.D. in engineering from Tokyo Institute of Technology in 2013. After graduation, he cofounded RIVERFIELD Inc. to develop and commercialize surgical robots. Following academic positions at Tokyo Institute of Technology and Tokyo KOSEN, he is currently an associate professor in the Faculty of Science and Engineering at Kindai University. His research focuses on surgical robots, motion control and teleoperation, and intelligent robot systems with physical AI. (d.haraguchi@mech.kindai.ac.jp)



Ryoga Ono received his associate degree from the National Institute of Technology, Tokyo College in 2021, his bachelor's degree from Toyohashi University of Technology in 2023, and his master's degree from the same university in 2025. He is currently working in industry. His research interests include biotechnology.